Acta of Bioengineering and Biomechanics
Vol. 27, No. 4, 2025

Original paper
DOI: 10.37190/abb/217836

Biomechanical evaluation of posterior deltoid exercises and kinematic trajectory modeling

QINGHUI ZHU, ZHIZI CHEN, LI FENG*

College of Home and Art Design, Northeast Forestry University, Harbin, Heilongjiang, China.

Purpose: This study aimed to quantitatively evaluate posterior deltoid activation during common strengthening exercises and establish a mathematical trajectory model to guide the control systems of upper-limb rehabilitation robots. *Methods*: Kinematic data were collected from ten healthy males performing the Bent-over Dumbbell Lateral Raise (BDLR), Standing Face Pull (SFP), and Bent-over Dumbbell Row (BDR). Inverse Kinematics and Static Optimization were performed using OpenSim musculoskeletal modeling to estimate muscle forces. The optimal exercise was identified through statistical comparison of Root Mean Square muscle forces. A continuous trajectory model using cubic polynomial fitting was derived from the biomechanically optimal movement to enable future robotic path planning. *Results*: The one-way ANOVA indicated a significant main effect of exercise type on muscle activation ($p < 0.001$). Tukey's HSD post-hoc tests revealed that both BDLR (58.591 N) and SFP (58.183 N) elicited comparable high activation levels with no statistically significant difference ($p > 0.05$). However, both exercises produced significantly higher muscle forces compared to BDR (47.911 N, $p < 0.001$). Although statistically equivalent to SFP, BDLR was selected as the target for trajectory modeling due to its kinematic suitability for end-effector based robotic rehabilitation. *Conclusions*: Bent-over dumbbell lateral raise demonstrates high efficacy for posterior deltoid recruitment. The kinematic trajectory model derived from optimal biomechanics provides a mathematically precise movement template for programming intelligent rehabilitation robots and training devices, enabling standardized execution of evidence-based strengthening protocols.

Key words: *posterior deltoid, muscle activation level, kinematic equations, exercise training*

1. Introduction

The posterior deltoid (PD) serves as the primary torque generator for shoulder horizontal abduction and extension [30]. Through the scapulohumeral force-couple mechanism, it plays a critical role in coordinating biomechanical force transmission during upper-limb push-pull actions [3], [10], [23]. Clinical studies indicate that PD weakness contributes significantly to shoulder muscle imbalances, with approximately 36% of shoulder injuries associated with its dysfunction [13], [15], [16], [27]. Consequently, strengthening the PD is not only essential for athletic performance but is also a cornerstone of shoulder rehabilitation and stability reconstruction.

Strength training is the primary intervention for PD development. While traditional exercises using free weights (e.g., dumbbells) are effective, they rely heavily on the patient's neuromuscular control and core stability [4]. In a rehabilitation context, this reliance poses risks of compensatory movements and injury [12], [17], [26]. Rehabilitation robotics has emerged as a promising solution, offering high repeatability, safety, and precise load management [29]. However, the effectiveness of a rehabilitation robot depends fundamentally on its control strategy, specifically the reference trajectory used to guide the end-effector [5], [8].

Current robotic rehabilitation protocols often rely on arbitrary geometric paths (e.g., straight lines or simple circles) rather than biomechanically validated human movement patterns [9], [21]. While trajectory planning

* Corresponding author: Li Feng, College of Home and Art Design, Northeast Forestry University, Harbin, Heilongjiang, China, e-mail: fengli86@nefu.edu.cn
Received: November 20th, 2025
Accepted for publication: February 5th, 2026

strategies exist for general upper-limb rehabilitation, protocols specifically targeting the PD often lack precision. There is a notable scarcity of mathematical trajectory models based on optimal biomechanics for isolating and strengthening this specific muscle to guide robotic control systems [31]. To design an effective robotic protocol, it is necessary to first identify the most biomechanically efficient exercise and then translate that human movement into a mathematical format executable by a robot [19], [28].

To identify the optimal exercise, rigorous biomechanical evaluation is required. Existing studies predominantly employ surface electromyography to measure localized muscle activation. While surface electromyography captures electrical signals, it struggles to quantitatively analyze deep muscle forces and joint moments [1]. In contrast, musculoskeletal modeling (e.g., OpenSim) utilizing Inverse Kinematics (IK) and Static Optimization (SO) allows for the estimation of individual muscle forces based on motion capture data, providing a deeper insight into joint mechanics [7].

Furthermore, bridging the gap between clinical motion data and robotic control presents an engineering challenge. Raw motion capture data is inherently discrete and noisy, making it unsuitable for direct input into robotic controllers. To achieve safe and smooth robotic actuation, transforming these discrete datasets into a continuous, differentiable mathematical representation is required [18], [20], [22], [25].

Therefore, this study aims to: (1) quantitatively compare PD activation during three common strengthening exercises – BDLR, SFP, and BDR – using OpenSim musculoskeletal modeling; (2) construct a mathematically precise trajectory model based on the optimal movement. This model provides a mathematically precise foundation for future robotic rehabilitation protocols, ensuring evidence-based and smooth execution of strengthening protocols.

2. Materials and methods

2.1. Muscle activation level experimental method

2.1.1. Data acquisition

Ten healthy, untrained male university students participated in this study (mean ± SD: age 21.4 ± 1.78 years, height 178.8 ± 2.62 cm, weight 78.8 ± 2.25 kg; detailed demographics in Appendix 1). All participants provided written informed consent, and the study protocol was approved by the Institutional Review Board. Subjects reported no history of shoulder injury within the past three months and refrained from strenuous exercise for 24 hours prior to testing.

Kinematic data were captured using an eight-camera BTS SMART-DX 3D motion capture system (BTS Bioengineering, Italy) at a sampling rate of 250 Hz. Reflective markers were placed on key anatomical landmarks, including the sternum, acromion, lateral epicondyle of the humerus, and the styloid process of the radius (detailed placement in Appendix 2).

Participants performed three exercises: BDLR, SFP, and BDR. To ensure consistency, participants were instructed to perform the concentric phase of each movement in a controlled manner.

2.1.2. OpenSim model

To quantify muscle forces, a musculoskeletal modeling approach was employed using OpenSim. The workflow consisted of four sequential steps: Model Scaling, IK, Residual Reduction Algorithm (RRA), and SO.

Scaling

A generic upper-limb musculoskeletal model was scaled to match the anthropometric dimensions of each participant based on static marker positions. The maximum marker error after scaling was kept below 2 cm, and the Root Mean Square (RMS) error was below 1 cm, ensuring geometric accuracy. In Figure 1, the detailed model scaling errors for the ten subjects is displayed, illustrating that both the coordinate error RMS (pink points) and maximum error (slate blue points) fell within acceptable thresholds.

IK

The experimental marker trajectories were input into the IK solver to resolve the generalized coordinates (joint angles) that best reproduced the subject's motion. This step transformed Cartesian marker data into joint space trajectories (θ_t). The computed joint kinematics, specifically the shoulder abduction angle and elbow flexion-extension angle across the three movement models, are visualized in Fig. 2.

RRA

RRA was applied to minimize the discrepancies between the experimental kinematics and the model's dynamic consistency. Residual forces and moments were minimized to improve the dynamic reliability of the simulation. The heatmap in Fig. 3 illustrates the distri-

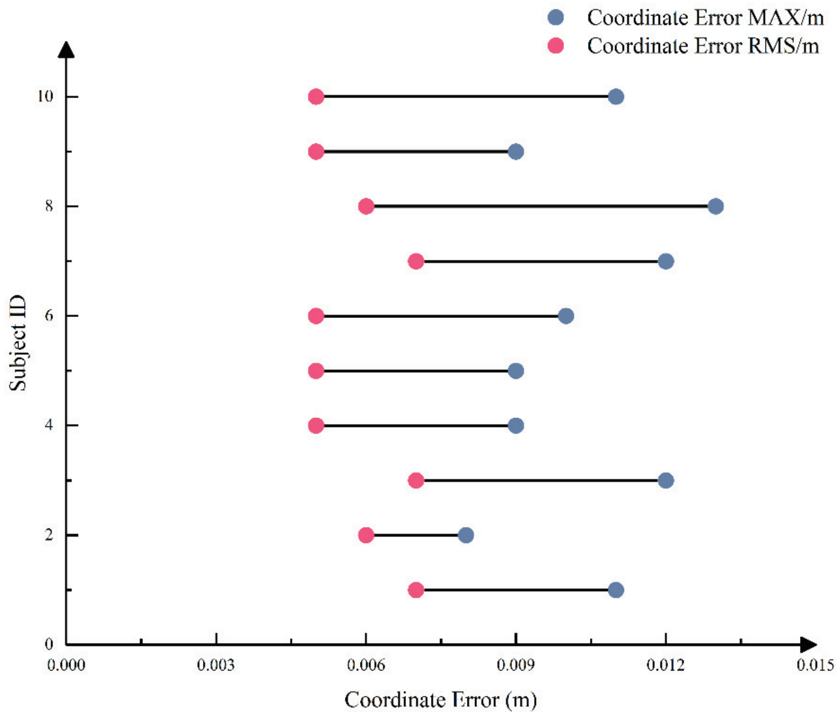

Fig. 1. The model scaling errors for the ten subjects, with pink points representing the coordinate error RMS and slate blue points representing the coordinate error MAX

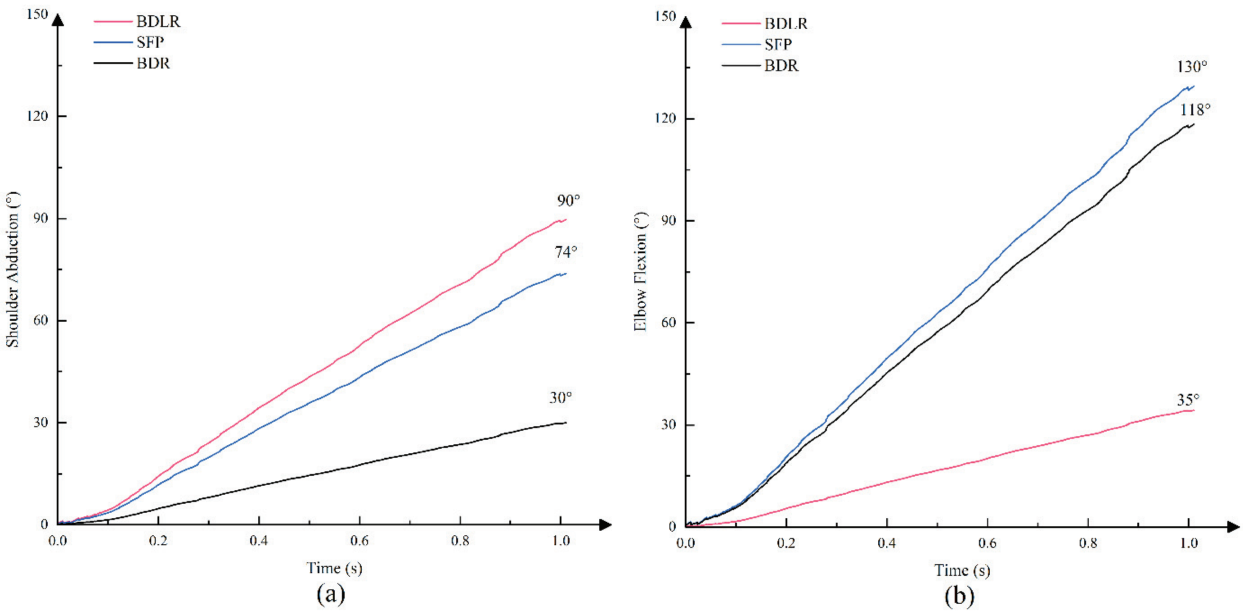

Fig. 2. The shoulder abduction angle and elbow flexion-extension angle outputs from inverse kinematics for the three movement models, where (a) represents the shoulder abduction angle and (b) represents the elbow flexion-extension angle

bution of these residual quantities across all subjects and exercises, confirming that the dynamic inconsistencies were effectively minimized.

SO

To estimate individual muscle forces, SO (an inverse dynamics-based method) was performed. This algorithm resolves the muscle redundancy problem by minimizing the sum of squared muscle activations at each time step, subject to the constraints of the force-length-velocity properties of the muscles. The output muscle force (F) of the PD was extracted for analysis.

To visually contextualize the biomechanical analysis, the OpenSim models corresponding to the three selected

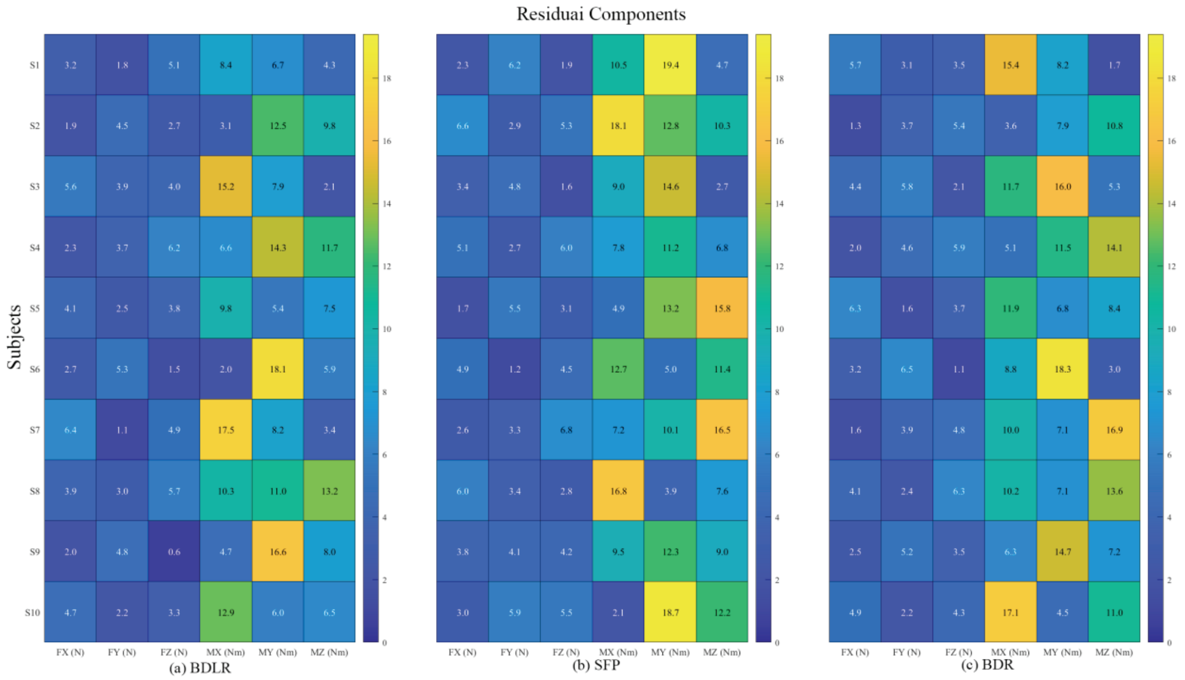

Fig. 3. Heatmap visualization of the Residual Reduction Algorithm (RRA) results.
The color intensity represents the magnitude of residual forces (FX, FY, FZ)
and moments (MX, MY, MZ) for each subject across the three exercises (BDLR, SFP, BDR)

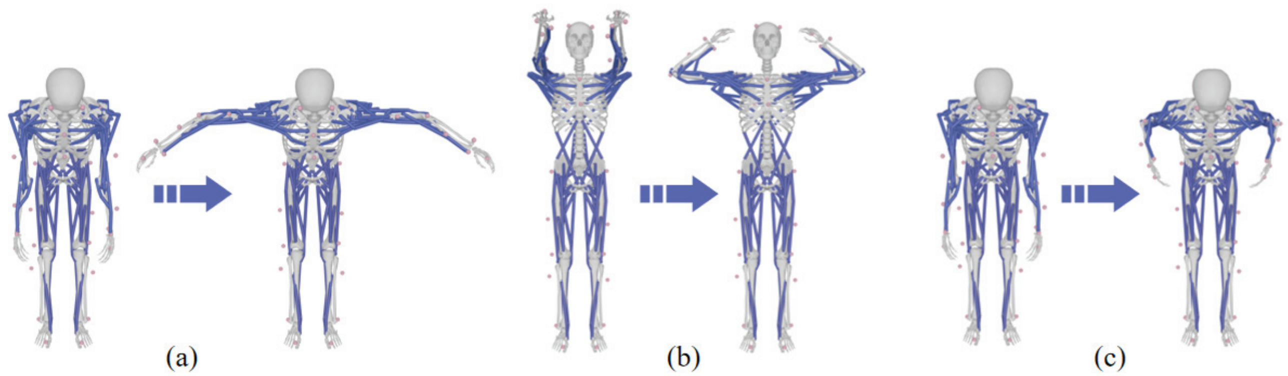

Fig. 4. Musculoskeletal simulation models of the three posterior deltoid exercises in OpenSim:
(a) BDLR; (b) SFP; (c) BDR. The arrows indicate the direction of the concentric phase

exercises are illustrated in Fig. 4. The diagrams depict the musculoskeletal configuration at both the initial and final postures for BDLR, SFP, and BDR.

2.2. Planar kinematic mapping and trajectory modeling

To bridge the gap between human biomechanics and robotic control, a mathematical trajectory model was developed based on the optimal exercise identified in the previous steps.

First, a planar kinematic mapping was established to describe the spatial relationship between the shoulder/elbow joint angles and the hand position (end-effector). Based on the anthropometric data (average upper arm length L_1 = 32.5 cm, forearm length L_2 = 27.5 cm) and the resolved joint angles (θ_1, θ_2) from IK, the position of the hand (X, Y) in the transverse plane was calculated using standard kinematic equations (Eq. (2)):

Although in Eq. (2) the geometric path is described, the raw kinematic data remains discrete. To convert this dataset into a control-ready format, a cubic polynomial fitting was applied to the calculated trajectory coordinates (X_t, Y_t). This fitting method was selected to generate a continuous function (Eq. (3)) with C^2 continuity, providing the necessary reference input for the robot's end-effector controller.

2.3. Statistical analysis

All muscle force data were normalized to 0–100% of the movement cycle to facilitate inter-subject comparison. RMS of the PD muscle force was calculated for each subject and exercise to quantify the overall activation level (Eq. (1)):

$$\mathrm{RMS} = \sqrt{\frac{1}{T}\int_0^T [F(t)]^2\,dt}\,. \tag{1}$$

Normality of the data was verified using the Shapiro–Wilk test. A one-way analysis of variance (ANOVA) was conducted to compare the RMS values across the three exercises (BDLR, SFP, BDR). To identify specific differences between group means, Tukey's Honest Significant Difference (HSD) post-hoc tests were performed. The effect size was calculated using Eta squared (η^2). All statistical analyses were performed with the significance level set at $p < 0.05$.

3. Results

3.1. Muscle activation result

3.1.1. Muscle force profiles (normalized)

The filtered muscle force profiles for the PD across the three exercises are illustrated in Fig. 5.

BDLR (Fig. 5a)

Peak force (112.816 N) at 0.041 s; secondary peak (99.823 N) at 0.749 s. Rapid post-peak decline indicated reliance on fast muscle recruitment.

SFP (Fig. 5b)

Peak force (111.641 N) occurred at 0.044 s, with a secondary peak (100.467 N) at 0.749 s. Similar to BDLR, significant fluctuations and rapid post-peak decline were observed, also suggesting rapid recruitment.

BDR (Fig. 5c)

Peak force (80.673 N) occurred at 0.75 s. Compared to BDLR and SFP, the force profile was relatively stable, indicating greater suitability for endurance training.

3.1.2. Comparative analysis and optimal exercise selection

The descriptive statistics for RMS muscle force are presented in Table 1. The individual RMS muscle force values for all 10 subjects, along with the group means and standard deviations, are detailed therein.

The one-way ANOVA revealed a statistically significant difference in PD activation among the three exercises (F (2, 27) = 10.635, $p < 0.001$). The effect size was large ($\eta^2 = 0.441$), indicating that exercise selection substantially influences muscle recruitment. Post-hoc comparisons using the Tukey HSD test revealed the following:

BDLR vs. SFP

The mean difference was 0.408 N. This difference was not statistically significant ($p > 0.05$), suggesting that both exercises provide comparable levels of muscle stimulation.

BDLR vs. BDR

BDLR elicited significantly higher muscle forces than BDR, with a mean difference of 10.680 N ($p < 0.001$).

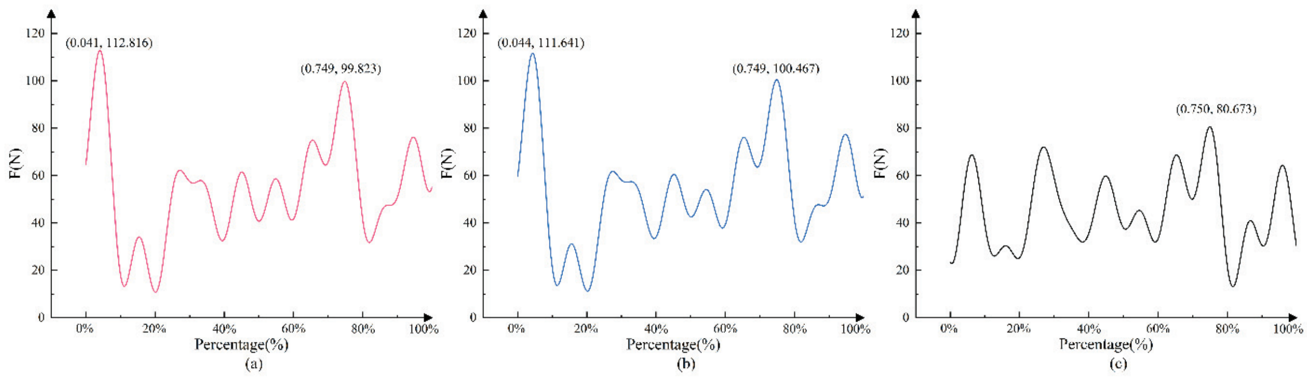

Fig. 5. The time-varying muscle force data curves for the three movement:
(a) representing the BDLR exercise; (b) the SFP exercise; (c) the BDR exercise

Table 1. Individual and mean RMS muscle forces [N] of the posterior deltoid for the three exercises ($n = 10$)

Subject ID	BDLR [N]	SFP [N]	BDR [N]
01	56.412	57.215	46.533
02	64.250	63.110	52.840
03	50.125	49.880	41.225
04	59.330	58.920	48.650
05	67.890	66.540	54.110
06	52.450	53.115	43.780
07	60.100	59.550	49.200
08	62.750	61.450	50.350
09	48.900	48.350	39.850
10	63.703	63.700	52.572
Mean ± SD	58.591 ± 6.106	58.183 ± 5.744	47.911 ± 4.766

SFP vs. BDR

SFP also produced significantly higher muscle forces than BDR, with a mean difference of 10.272 N ($p < 0.001$).

Selection Rationale: Although statistical analysis indicated that BDLR and SFP are equivalent in terms of muscle activation efficacy, BDLR was selected as the optimal target for kinematic trajectory modeling based on engineering criteria for rehabilitation robotics. This decision was driven by the kinematic simplicity of BDLR, which predominantly follows a planar arc trajectory in the transverse plane, whereas SFP involves complex multi-planar coupling (abduction combined with external rotation). Consequently, the planar trajectory of BDLR is geometrically simpler to model and safer to control using a robotic end-effector. Furthermore, regarding safety, the BDLR movement vector is directed away from the body, which significantly minimizes collision risks compared to the face-directed path inherent to the SFP.

3.2. Kinematic modelling for robotic control

3.2.1. Planar kinematic mapping

Based on the selected BDLR exercise, a planar kinematic model was established to map the joint space to the Cartesian workspace. The BDLR coordinate system designated the shoulder joint as the origin (0, 0). The Y-axis was vertically upward (opposing gravity), and the X-axis extended horizontally to the right (Fig. 6). The general kinematic equation is defined as (Eq. (2)):

$$\begin{cases} x(t) = L_1 \sin\theta_1(t) + L_2 \sin(\theta_1(t) + \theta_2(t)) \\ y(t) = -[L_2 \cos\theta_1(t) + L_2 \cos(\theta_1(t) + \theta_2(t))] \end{cases}, \quad (2)$$

where L_1 represents the upper arm length (unit: cm); L_2 represents the forearm length (unit: cm); θ_1 denotes the shoulder abduction angle (in radians); θ_2 denotes the elbow flexion-extension angle (in radians).

Based on GB/T 10 000 – 1988, median adult limb lengths were used: L_1 = 32.5 cm (upper arm) and L_2 = 27.5 cm (forearm). Substituting these parameters into Eq. (2) yields the specific kinematic relationship for the BDLR movement:

$$\begin{cases} x(t) = 32.5 \sin\theta_1(t) + 27.5 \sin(\theta_1(t) + \theta_2(t)) \\ y(t) = -[32.5 \cos\theta_1(t) + 27.5 \cos(\theta_1(t) + \theta_2(t))] \end{cases}. \quad (3)$$

Using the averaged joint angle data (θ_1, θ_2) from the OpenSim IK results, the discrete end-effector (hand) coordinates were calculated. The resulting data points are listed in Table 2.

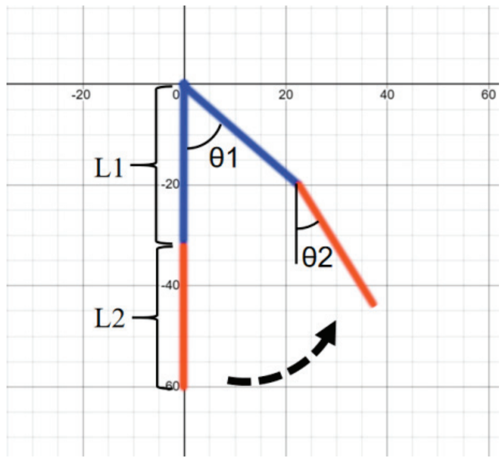

Fig. 6. Planar coordinate definition for BDLR exercise: (0, 0) in the figure corresponds to the human shoulder joint; (0, $-(L_1 + L_2)$) corresponds to the initial state of BDLR

Table 2. End-effector (hand) position coordinates (cm)

Time [s]	$X(t)$	$Y(t)$
0	0.000	–60.000
0.1	5.439	–59.717
0.2	17.408	–57.344
0.3	29.047	–52.177
0.4	39.937	–43.990
0.5	48.445	–32.667
0.6	53.100	–21.854
0.7	56.190	–16.464
0.8	57.920	–14.134
0.9	58.645	–12.055
1.0	57.982	–11.719

3.2.2. Continuous trajectory modelling (polynomial fitting)

Using the averaged joint angle data (converted to radians) from the OpenSim Inverse Kinematics outputs, the end-effector coordinates were calculated via the planar kinematic model (Eq. (3)). For the 0–1 s movement interval (0.1 s time step), 11 sets of discrete data points were extracted (Table 2).

To obtain a continuous mathematical representation suitable for robotic control, this discrete trajectory data (X_{real}, Y_{real}) was fitted using cubic polynomial functions. The spatial motion was decomposed into horizontal (X) and vertical (Y) components as follows (Eq. (4)):

$$\begin{cases} X_{(t)} = a_0 + a_1 t + a_2 t^2 + a_3 t^3 \\ Y_{(t)} = b_0 + b_1 t + b_2 t^2 + b_3 t^3 \end{cases}, \tag{4}$$

where t is time (s), and a_0, a_1, a_2, a_3, b_0, b_1, b_2, b_3 are coefficients.

The specific values of these coefficients were determined using the least squares method to minimize the fitting error. The matrix formulations for the solution are expressed as follows:

$$\begin{bmatrix} 1 & t_1 & t_1^2 & t_1^3 \\ 1 & t_2 & t_2^2 & t_2^3 \\ \vdots & \vdots & \vdots & \vdots \\ 1 & t_n & t_n^2 & t_n^3 \end{bmatrix} \begin{bmatrix} a_0 \\ a_1 \\ a_2 \\ a_3 \end{bmatrix} = \begin{bmatrix} x_{(t_1)} \\ x_{(t_2)} \\ \vdots \\ x_{(t_n)} \end{bmatrix}, \tag{5}$$

$$\begin{bmatrix} 1 & t_1 & t_1^2 & t_1^3 \\ 1 & t_2 & t_2^2 & t_2^3 \\ \vdots & \vdots & \vdots & \vdots \\ 1 & t_n & t_n^2 & t_n^3 \end{bmatrix} \begin{bmatrix} b_0 \\ b_1 \\ b_2 \\ b_3 \end{bmatrix} = \begin{bmatrix} y_{(t_1)} \\ y_{(t_2)} \\ \vdots \\ y_{(t_n)} \end{bmatrix}. \tag{6}$$

Solving these matrices yielded the following coefficients: $a_0 = 0$; $a_1 = 91.474$; $a_2 = 36.667$; $a_3 = -71.789$; $b_0 = -60.000$; $b_1 = -29.846$; $b_2 = 254.580$; $b_3 = -177.924$.

Substituting these values into Eq. (4) yields the final continuous trajectory equation for the BDLR movement (Eq. (7)):

$$\begin{cases} X_{(t)} = 91.474t + 36.667t^2 - 71.789t^3 \\ Y_{(t)} = -60 - 29.846t + 254.580t^2 - 177.924t^3 \end{cases}. \tag{7}$$

To validate the fitted equations, time values t (0, 0.1, ... 1.0 s) were substituted into Eq. (7) to generate predicted coordinates (X_{pred}, Y_{pred}) (Table 3). These were compared against the actual values (X_{real}, Y_{real}) from Table 2 using error-bar visualizations (Fig. 7).

In Figure 7, the blue solid line represents real values, the red dashed line represents predicted values, and blue error bars indicate prediction errors. Predicted values closely matched real values at most time points. The maximum error in X was 4.003 cm at 0.1 s, and in Y was 2.836 cm at 0.6 s. Coefficients of determination (R^2) calculated between real and predicted values were 0.9920 (X-direction) and 0.9944 (Y-direction).

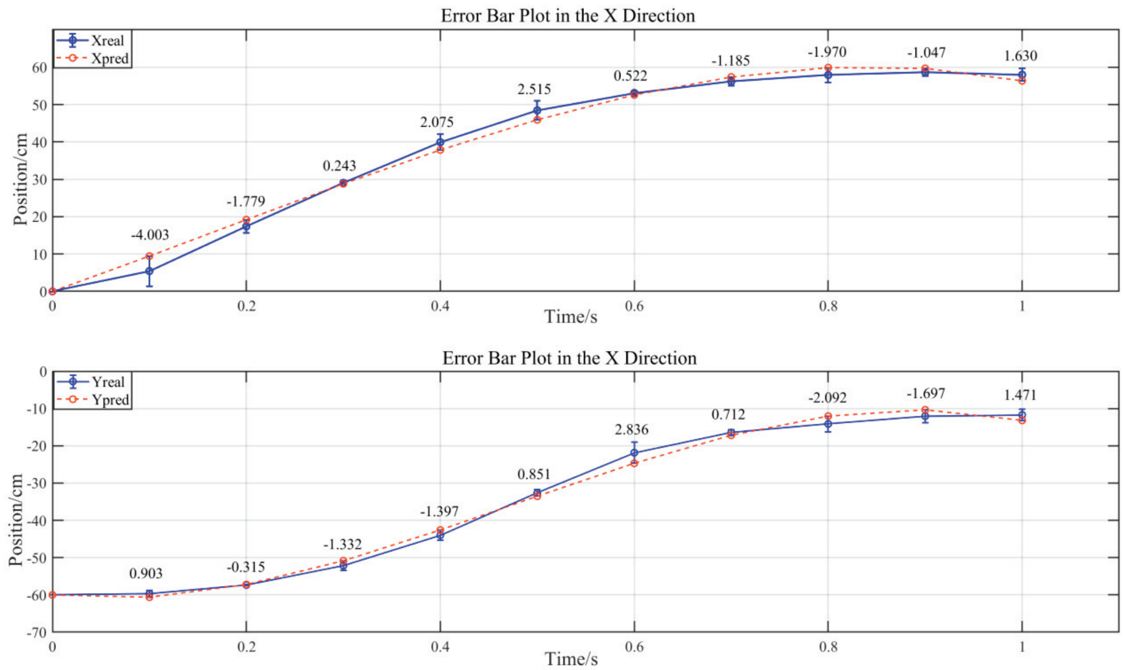

Fig. 7. The error bar plots for the end-effector trajectory equation fitting of the BDLR: the upper panel displays the errors between the real and predicted values in the X direction, and the lower panel displays the errors between the real and predicted values in the Y direction

The coefficients of determination ($R^2 > 0.99$) confirm that the cubic polynomial provides a high-fidelity mathematical representation of the human movement. This indicates that the transition from discrete motion capture data to a continuous analytical function was achieved without significant signal loss or distortion. Consequently, this function can serve as a reliable reference for the robot controller, ensuring that the machine precisely replicates the intended biomechanical path.

Table 3. Predicted values in the *X* and *Y* directions

Time [s]	X_{pred} [cm]	Y_{pred} [cm]
0	0.000	–60.000
0.1	9.442	–60.620
0.2	19.187	–57.209
0.3	28.804	–50.845
0.4	37.862	–42.593
0.5	45.930	–33.518
0.6	52.578	–24.690
0.7	57.375	–17.176
0.8	59.890	–12.042
0.9	59.692	–10.358
1.0	56.352	–13.190

4. Discussions

4.1. Biomechanical mechanisms of muscle activation

The results demonstrated that the PD activation during BDLR (58.591 N) and SFP (58.183 N) was substantially higher than during BDR (47.911 N). This finding aligns with the functional anatomy of the shoulder complex. The PD is the primary agonist for horizontal abduction (involved in BDLR and SFP) and a synergist for extension (involved in BDR).

During the BDR exercise, the movement vector involves significant shoulder extension, where the Latissimus Dorsi acts as a powerful prime mover, potentially creating a “shielding effect” that reduces the load demand on the PD [11]. In contrast, the BDLR involves pure horizontal abduction in the transverse plane. In this position, the gravity vector acts perpendicularly to the humerus throughout the range of motion, creating a maximal external torque that must be counteracted specifically by the PD. This isolation effect explains the higher force values observed in BDLR and SFP compared to the multi-joint rowing movement.

4.2. Implications for rehabilitation robotics

A key finding of the statistical analysis was that the difference in RMS muscle force between BDLR and SFP was minimal (~0.4 N) and not statistically significant ($p > 0.05$). While both exercises are clinically effective, BDLR was selected as the optimal template for robotic trajectory modeling based on engineering and safety criteria.

From the perspective of kinematic simplicity, the SFP involves a complex coupling of shoulder abduction, external rotation, and elbow flexion, requiring a robot with high degrees of freedom (DOF) and complex joint coordination algorithms. Conversely, the BDLR trajectory is predominantly planar (transverse plane). This geometric simplicity reduces the computational burden on the robot controller and minimizes the risk of kinematic singularities [2].

Regarding the safety profile, in the SFP movement, the hand is pulled towards the face. In a robotic rehabilitation setting, this trajectory poses a potential collision risk if the control system fails or if the patient spasms. The BDLR trajectory moves away from the body’s centerline, offering a higher inherent safety margin for human-robot interaction [6], [24].

4.3. Utility of the polynomial trajectory model

The derivation of the cubic polynomial equation provides an effective mathematical framework for translating biomechanics into robotic control. While raw motion capture data describes the position, it is discrete and contains high-frequency noise. Directly using such data for robotic control can lead to discontinuous velocity and acceleration profiles, causing mechanical jitter. The fitted polynomial model ($R^2 > 0.99$) converts the biological data into a continuous, differentiable mathematical function. This provides three critical engineering advantages. First, regarding smooth actuation, the model allows the robot controller to generate smooth feedforward velocity and acceleration signals, ensuring comfortable and jerk-free movement for the patient. Second, concerning data compression, it reduces large discrete datasets into a few coefficients, optimizing storage in embedded controllers. Finally, with respect to time scaling, the parametric nature of the function allows therapists to easily adjust the speed of rehabilitation without altering the geometric path, accommodating patients at different recovery stages.

4.4. Limitations

Several limitations should be noted. First, the sample size (N = 10) was relatively small and consisted of healthy males; future studies should include females and patients with shoulder pathology to validate the trajectory's universality. Second, muscle forces were estimated using SO without direct electromyography (EMG) validation; however, the observed results are consistent with the findings of Kang et al. [14], supporting the biomechanical validity of the simulation. Third, the trajectory was modeled in a 2D plane for simplification; while sufficient for BDLR, a 3D model would be required for more complex movements. Fourth, it is acknowledged that the absolute difference in RMS muscle force between BDLR and SFP was marginal (~0.4 N). While BDLR was selected for modeling, this decision was driven primarily by robotic control constraints (kinematic simplicity) rather than a distinct physiological superiority over SFP. Future studies should investigate whether this minor force difference translates to long-term clinical benefits.

5. Conclusions

This study quantitatively evaluated PD activation during three strengthening exercises and established a kinematic model for the optimal movement to support rehabilitation robotics. The key findings are:

Three key findings emerge from this study. First, regarding exercise selection, both BDLR and SFP elicited comparable high muscle forces (RMS: 58.591 N and 58.183 N, respectively), significantly surpassing BDR (47.911 N). Second, in terms of robotic applicability, although statistically equivalent to SFP, the BDLR was identified as the superior candidate for robotic implementation due to its open-chain kinematic simplicity and enhanced safety profile (moving away from the body). Finally, concerning trajectory modeling, a cubic polynomial trajectory model was successfully derived from the optimal biomechanical data (R^2 > 0.99). This model provides a standardized reference trajectory for programming intelligent rehabilitation robots, enabling evidence-based PD strengthening while ensuring safe human-robot interaction.

Competing interests

The authors declare that they have no known competing financial interests or personal relationships that could have appeared to influence the work reported in this paper. The authors confirm that this manuscript has not been published previously and is not currently under consideration for publication elsewhere.

Credit authorship contribution statement

Qinghui Zhu – the execution of research; the interpretation of data:

Zhizi Chen – the statistical analysis,

Li Feng – the preparation of the research program.

Data availability statement

The datasets supporting this study are available from the corresponding author upon reasonable request.

References

[1] Ao D., Shourijeh M.S., Patten C., Fregly B.J., *Evaluation of Synergy Extrapolation for Predicting Unmeasured Muscle Excitations from Measured Muscle Synergies*, Front. Comput. Neurosci., 2020, 14, 588943.

[2] Aribowo W., Terashima K., *Cubic Spline Trajectory Planning and Vibration Suppression of Semiconductor Wafer Transfer Robot Arm*, International Journal of Automation Technology, 2014, 8, 265–274.

[3] Camargo P.R., Avila M.A., Alburquerque-Sendín F., Asso N.A., Hashimoto L.H., Salvini T.F., *Eccentric training for shoulder abductors improves pain, function and isokinetic performance in subjects with shoulder impingement syndrome: a case series*, Brazilian Journal of Physical Therapy, 2012, 16 (1), 74–83.

[4] Campos Y.A.C. et al., *Different Shoulder Exercises Affect the Activation of Deltoid Portions in Resistance-Trained Individuals*, Journal of Human Kinetics, 2020, 75 (1), 5–14.

[5] Colombo G., Joerg M., Schreier R., Dietz V., *Treadmill training of paraplegic patients using a robotic orthosis*, J. Rehabil. Res. Dev., 2000, 37 (6), 693–700.

[6] Cooney M., Zanlungo F., Nishio S., Ishiguro H., *Designing a flying humanoid robot (FHR): Effects of flight on interactive communication*, IEEE RO-MAN, 2012, 364–371.

[7] Delp S.L. et al., *OpenSim: Open-Source Software to Create and Analyze Dynamic Simulations of Movement*, IEEE Transactions on Biomedical Engineering, 2007, 54 (11), 1940–1950.

[8] Du Y., Wang H., Qiu S., Yao W., Xie P., Chen X., *An Advanced Adaptive Control of Lower Limb Rehabilitation Robot*, Front. Robot AI, 2018, 5, 116.

[9] Duschau-Wicke A., Von Zitzewitz J., Caprez A., Lunenburger L., Riener R., *Path control: a method for patient--cooperative robot-aided gait rehabilitation*, IEEE Trans. Neural. Syst. Rehabil. Eng., 2010, 18 (1), 38–48.

[10] Ertuğrul Y., Sevgi Sevi Y., *Scapular stabilization exercise training improves treatment effectiveness on shoulder pain, scapular dyskinesis, muscle strength, and function in patients with subacromial pain syndrome: A randomized controlled trial*, Journal of Bodywork and Movement Therapies, 2024, 37, 101–108.

[11] FISCHER J. et al., *Impact of different ranges of motion in the prone barbell row on muscle excitation*, Journal of Electromyography and Kinesiology, 2025, 83, 103025.

[12] HUG F., GOUPILLE C., BAUM D., RAITERI B.J., HODGES P.W., TUCKER K., *Nature of the coupling between neural drive and force-generating capacity in the human quadriceps muscle*, Proceedings of the Royal Society B: Biological Sciences, 2015, 282 (1819), 20151908.

[13] ISHIKAWA H. et al., *Rotator cuff muscle imbalance associates with shoulder instability direction*, Journal of Shoulder and Elbow Surgery, 2023, 32 (1), 33–40.

[14] KANG M.H., OH J.S., JANG J.H., *Differences in Muscle Activities of the Infraspinatus and Posterior Deltoid during Shoulder External Rotation in Open Kinetic Chain and Closed Kinetic Chain Exercises*, J. Phys. Ther. Sci., 2014, 26 (6), 895–897.

[15] KIDO T., ITOI E., LEE S.B., NEALE P.G., AN K.N., *Dynamic stabilizing function of the deltoid muscle in shoulders with anterior instability*, Am. J. Sports Med., 2003, 31 (3), 399–403.

[16] KOLBER M.J., BEEKHUIZEN K.S., CHENG M.S.S., HELLMAN M.A., *Shoulder Injuries Attributed to Resistance Training: A Brief Review*, Journal of Strength and Conditioning Research, 2010, 24 (6), 1696–1704.

[17] LI H., ZHAO G., ZHOU Y., CHEN X., JI Z., WANG L., *Relationship of EMG/SMG features and muscle strength level: an exploratory study on tibialis anterior muscles during plantarflexion among hemiplegia patients*, BioMedical Engineering OnLine, 2014, 13, 5.

[18] LIU G., SUN W., LI P., *Motion capture and AR based programming by demonstration for industrial robots using handheld teaching device*, Sci. Rep., 2024, 14 (1), 23259.

[19] MA J.W., GAO S., YAN H.T., LV Q., HU G.Q., *A new approach to time-optimal trajectory planning with torque and jerk limits for robot*, Robotics and Autonomous Systems, 2021, 140, 103744.

[20] MACFARLANE S., CROFT E.A., *Jerk-bounded manipulator trajectory planning: design for real-time applications*, IEEE Transactions on Robotics and Automation, 2003, 19 (1), 42–52.

[21] MARCHAL-CRESPO L., REINKENSMEYER D.J., *Review of control strategies for robotic movement training after neurologic injury*, J. Neuroeng. Rehabil., 2009, 6, 20.

[22] MEMAR ARDESTANI M., YAN H., *Noise Reduction in Human Motion-Captured Signals for Computer Animation based on B-Spline Filtering*, Sensors (Basel), 2022, 22 (12), 19.

[23] MORODER P. et al., *Characteristics of functional shoulder instability*, Journal of Shoulder and Elbow Surgery, 2020, 29 (1), 68–78.

[24] NISAL MENUKA G., DEEPANA I., WEIGEL M., ANUSHA W., *So Predictable! Continuous 3D Hand Trajectory Prediction in Virtual Reality*, Honda Research Institute Europe GmbH, 2021, 3472749.

[25] PIAZZI A., VISIOLI A., *Global minimum-jerk trajectory planning of robot manipulators*, IEEE Transactions on Industrial Electronics, 2000, 47 (1), 140–149.

[26] RABELLO R. et al., *Activation of the three deltoid muscle portions during common strengthening exercises: A systematic review*, Journal of Bodywork and Movement Therapies, 2024, 40, 1309–1325.

[27] ROMERO S. et al., *Trajectory Planning for Robotic Manipulators in Automated Palletizing: A Comprehensive Review*, Robotics, 2025, 14 (1), 5.

[28] WANG H., CHEN L., XU G., LIU H., *Biomechanical effects of deltoid muscle atrophy on rotator cuff tissue: a finite element study*, Scientific Reports, 2024, 14 (1), 17592.

[29] XIE S. et al., *Predictive Control for an Ankle Rehabilitation Robot Using Differential Evolution Optimization Algorithm-Based Fuzzy NARX Model*, IEEE Transactions on Neural Systems and Rehabilitation Engineering, 2025, 33, 1886–1895.

[30] YAN Y., TANG M., WANG W., ZHANG Y., AN B., *Trajectory tracking control of wearable upper limb rehabilitation robot based on Laguerre model predictive control*, Robotics and Autonomous Systems, 2024, 179, 104745.

[31] YEŞILYAPRAK S.S., *Chapter 11 – Kinesiology of the shoulder complex, in Comparative Kinesiology of the Human Body*, Academic Press, 2020, 157–190.

[32] ZHOU C. et al., *Development of an upper limb muscle strength rehabilitation assessment system using particle swarm optimisation*, Front. Bioeng. Biotechnol., 2025, 13, 1619411.

Appendix 1. Subject details

Number	Gender	Age	Height [cm]	Weight [kg]
01	male	19	180	80
02	male	23	178	77
03	male	22	177	79
04	male	22	181	79
05	male	22	183	82
06	male	21	175	74
07	male	25	179	81
08	male	21	182	80
09	male	19	176	78
10	male	20	177	78

Appendix 2. Anatomical marker placement

Marker code	Anatomical location	Quantity
LDMp/RDMp	Mid-belly of posterior deltoid	2
LSCAP/RSCAP	Midpoint of scapular spine	2
LINF/RINF	Inferior angle of scapula	2
LUPA/RUPA	Midpoint of posterior upper arm	2
T5/T8	Spinous process of T5/T8 vertebra	2
LSHO/RSHO	Acromion	2
LELB/RELB	Lateral epicondyle of humerus	2
C7	Spinous process of C7 vertebra	1
STRN	Suprasternal notch	1
CLAV	Manubrium sterni	1
LTHI/RTHI	Midpoint of lateral thigh	2
LKNE/RKNE	Lateral femoral epicondyle	2
LANK/RANK	Lateral malleolus	2
LWRB/RWRB	Ulnar styloid process	2
LMTP/RMTP	Dorsal aspect of 1st metatarsophalangeal joint	2

Appendix 3. Motion capture coordinate errors

Movement	Coordinate error RMS/m	Coordinate error MAX/m
01	0.007	0.011
02	0.006	0.008
03	0.007	0.012
04	0.005	0.009
05	0.005	0.009
06	0.005	0.010
07	0.007	0.012
08	0.006	0.013
09	0.005	0.009
10	0.005	0.011

Appendix 4. RRA of different movements in 10 subjects

(a) BDLR

Number	*FX* [N]	*FY* [N]	*FZ* [N]	*MX* [Nm]	*MY* [Nm]	*MZ* [Nm]
1	3.2	1.8	5.1	8.4	6.7	4.3
2	1.9	4.5	2.7	3.1	12.5	9.8
3	5.6	3.9	4.0	15.2	7.9	2.1
4	2.3	3.7	6.2	6.6	14.3	11.7
5	4.1	2.5	3.8	9.8	5.4	7.5
6	2.7	5.3	1.5	2.0	18.1	5.9
7	6.4	1.1	4.9	17.5	8.2	3.4
8	3.9	3.0	5.7	10.3	11.0	13.2
9	2.0	4.8	0.6	4.7	16.6	8.0
10	4.7	2.2	3.3	12.9	6.0	6.5

(b) SFP

Number	*FX* [N]	*FY* [N]	*FZ* [N]	*MX* [Nm]	*MY* [Nm]	*MZ* [Nm]
1	2.3	6.2	1.9	10.5	19.4	4.7
2	6.6	2.9	5.3	18.1	12.8	10.3
3	3.4	4.8	1.6	9.0	14.6	2.7
4	5.1	2.7	6.0	7.8	11.2	6.8
5	1.7	5.5	3.1	4.9	13.2	15.8
6	4.9	1.2	4.5	12.7	5.0	11.4
7	2.6	3.3	6.8	7.2	10.1	16.5
8	6.0	3.4	2.8	16.8	3.9	7.6
9	3.8	4.1	4.2	9.5	12.3	9.0
10	3.0	5.9	5.5	2.1	18.7	12.2

(c) BDR

Number	FX [N]	*FY* [N]	*FZ* [N]	*MX* [Nm]	*MY* [Nm]	*MZ* [Nm]
1	5.7	3.1	3.5	15.4	8.2	1.7
2	1.3	3.7	5.4	3.6	7.9	10.8
3	4.4	5.8	2.1	11.7	16.0	5.3
4	2.0	4.6	5.9	5.1	11.5	14.1
5	6.3	1.6	3.7	11.9	6.8	8.4
6	3.2	6.5	1.1	8.8	18.3	3.0
7	1.6	3.9	4.8	10.0	7.1	16.9
8	4.1	2.4	6.3	10.2	7.1	13.6
9	2.5	5.2	3.5	6.3	14.7	7.2
10	4.9	2.2	4.3	17.1	4.5	11.0

Appendix 5. Shoulder and elbow kinematics during BDLR

Time [s]	θ_1	θ_2
0	0	0
0.1	0.077	0.030
0.2	0.249	0.095
0.3	0.416	0.159
0.4	0.601	0.230
0.5	0.761	0.291
0.6	0.915	0.350
0.7	1.084	0.414
0.8	1.235	0.473
0.9	1.418	0.543
1.0	1.569	0.601